Hadronic Final States of Deep-Inelastic Processes in Simple Quark-Parton Models

John Kogut and D. K. Sinclair

Institute for Advanced Study, Princeton, New Jersey 08540

Leonard Susskind[*]

University of Tel Aviv, Ramat Aviv, Tel Aviv, Israel

(Received 12 December 1972)

Bjorken and Feynman have suggested a quark-parton-model approach to predicting the final-state hadron spectra in deep-inelastic processes. Since the final-state interaction in their approach is characterized by short-range correlations in rapidity, it is natural to ask whether parton models with final-state interactions based on conventional multiperipheral dynamics might provide realizations of their picture. This is found to be untrue. We argue by studying perturbation-theory models (ϕ^3 and cutoff vector-gluon ladder models) and by formulating a rather general intuitive space-time argument that in naive parton models of this type one cannot avoid the appearance of isolated-quark quantum numbers in the final state. In the $\lambda\phi^3$ models the final-state interaction always vanishes in the deep-inelastic region (as well as in the high-energy annihilation region) regardless of the size of λ. In the vector-gluon model, the final-state interaction does not vanish asymptotically, but the struck quark parton cannot exchange its charge with the target fragments. The character of parton dynamics necessary to realize the Bjorken-Feynman picture is discussed.

I. INTRODUCTION

Recently Bjorken[1] and co-workers,[2] and Feynman[3] and co-workers[4] have proposed a quark-parton-model approach to understanding the final hadronic states in deep-inelastic processes. It is the purpose of the present article to ask whether simple parton models based on conventional dynamical mechanisms lead to conclusions in agreement with the Bjorken-Feynman expectations.[1,2] We consider perturbation-theoretic models which scale in the deep-inelastic region and consider final-state parton-parton interactions which are multiperipheral in character. The Bjorken-Feynman picture does not emerge. In particular, if partons were quarks, then conventional multiperipheral mechanisms could not prohibit their production in deep-inelastic processes. We speculate briefly on what new features parton-parton interactions would need in order to realize the Bjorken-Feynman picture.[1,3]

Our motivation for studying this problem is the intriguing possibility that partons are bare quarks. If that were the case, then the parton model would provide a simple realization of many current-algebra sum rules and might really be of fundamental significance. However, given this hypothesis, the model must face the question as to why quark quantum numbers are not observed experimentally as the products of deep-inelastic reactions. Traditionally, this problem is not considered seriously in discussions of the reaction $e + p \rightarrow e +$ anything, where no final-state hadrons are ob-

served. The rationale for neglecting this problem is the argument that the parton system after collision converts to hadrons with unit probability. Hence, an understanding of the final-state interactions responsible for the conversion of quarks to hadrons is not necessary in understanding the function νW_2. However, experiments are now beginning to study the final states in deep-inelastic collisions; so this problem must be faced. In fact, a clear picture of the dynamics which converts the quark partons to real hadrons is necessary before one can claim that the quark-parton model is an approximate representation of a real theory and not just a mnemonic device. Recently these problems were considered to some extent in Refs. 1–3, and a quark-parton picture of hadronic final states was introduced. Many interesting and very reasonable predictions were then deduced from this point of view. It is the purpose of this article, however, to consider critically some of these ideas both with the use of intuitive infinite-momentum arguments and the study of graphs in perturbation-theoretic realizations of the parton model. We shall see that to realize the Bjorken-Feynman model appears to require dynamical mechanisms which fall outside simple relativistic perturbation-theory or multiperipheral realizations of the parton model.

This article is organized as follows. In Sec. II we briefly sketch the quark-parton picture of final-state interactions in deep-inelastic processes. In Sec. III a space-time argument is presented which motivates our suspicion that typical dynamics

based solely on short-range correlations in momentum space cannot implement the physical picture of Sec. II. Also included in Sec. III are additional perturbative arguments in support of this view. Section IV summarizes the detailed, straightforward calculations of the physical effects discussed in Sec. III. This is done in the context of several perturbation-theoretic parton models. The explicit calculations are relegated to several appendixes. Finally, in Sec. V. we discuss the implications of these results and speculate upon possible additional dynamical effects which would have to be incorporated into a quark-parton model to implement the ideas of Sec. II.

II. QUARK-PARTON MODEL AND FINAL STATES

Before proceeding with the substance of this article, we should review briefly the quark-parton picture of final states as developed by Bjorken and co-workers,[1,2] and Feynman and co-workers.[3,4] This discussion is borrowed in large part from Ref. 2. Consider deep-inelastic electron scattering in the over-all center-of-mass frame. Before the collision the hadron moving in the $+z$ direction is viewed as an assembly of partons (black dots in Fig. 1) each possessing small momentum transverse to the z axis. The electron (open circle in Fig. 1) approaches in the $-z$ direction. The electron then scatters (single-photon exchange) violently off a charged parton which is given a large momentum transverse to the initial beam direction (Fig. 2). This configuration of partons must now evolve into an assembly of ordinary hadrons which are observed in the lab. In this process the struck parton's quark quantum numbers must also leak back to the partons left behind.[5]

In guessing how the struck parton evolves into hadrons one evokes a central assumption of the parton model: that only partons possessing small relative subenergies interact significantly. This assumption plays an important role in establishing the impulse approximation for $e + p \rightarrow e + \text{anything}$; so it is natural to assume that this same dynamical assumption also applies to the evolution of the struck parton in Fig. 2. Since the struck parton
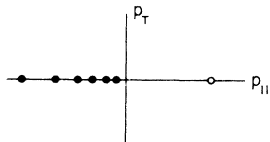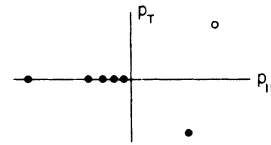

FIG. 2. Configuration of partons just after the deep-inelastic collision.

has a large subenergy when combined with any other parton in Fig. 2, one then argues that it initially evolves independently of the partons left behind. Furthermore, the evolution of that parton into other partons should be dominated by subprocesses each of which only involves partons nearby in momentum space. This strongly suggests that the struck parton interacts with those left behind by forming a cascade of partons until Fig. 2 has evolved into Fig. 3. The last partons in this cascade then have low relative subenergies when combined with those left behind, and there will be considerable interaction at this point. It is through this interaction that the fractional charge originally carried by the struck parton may be "neutralized" by the fractional charge of the fragments of the target.[5]

The final ingredient in this picture is the relation between the parton configuration in Fig. 3 and an actual final state of hadrons. Again, since only partons nearby in phase space are assumed to interact significantly, it is sensible to assume that only partons nearby in phase space combine to form an outgoing hadron. Thus, Fig. 3 is replaced by Fig. 4, for example.

From these assumptions, in particular the assumption that only partons nearby in phase space interact significantly, one can proceed to postulate the existence of parton fragmentation functions. The argument for this parallels the argument for Feynman-Yang scaling in hadron-hadron collisions at high energy.[6] These functions, which give the probability that a struck parton of type i fragments into a hadron of type c with a fraction x of the struck parton's momentum, are denoted $G_{ic}(x)$ in Ref. 2. From our discussion above, one expects that $G_{ic}(x) \sim c_{ic}/x$ for small x. Then it follows that multiplicities in e^+e^- collisions, say, at center-of-mass energy E, should grow as $\ln E$. This be-

FIG. 1. Configuration of partons in phase space immediately before a deep-inelastic collision. The open circle is the incident electron.
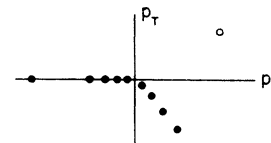

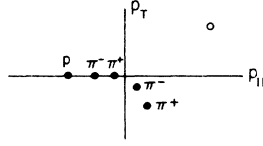FIG. 3. Configuration of partons long after the deep-inelastic collision.

FIG. 4. A possible configuration of hadrons in phase space resulting from the parton configuration of Fig. 3.

havior can also be read directly from Figs. 1–4. The functions G_{ic} clearly define a program for predicting, analyzing, and interpreting the experimental data on deep-inelastic processes such as $e + p \rightarrow e + \text{hadron} + \text{anything}$, $e^+ + e^- \rightarrow \text{hadron} + \text{anything}$, $p + p \rightarrow \text{hadron}$ (at large p_T) + anything, etc. In this article we are interested in making a critical analysis of this approach. In particular, we wish to know whether conventional dynamics, which only couples together partons which are nearby in momentum space, can keep quarks from being produced in deep-inelastic reactions.

III. INTUITIVE DISCUSSION OF FINAL STATES IN THE QUARK-PARTON MODEL

A. Space-Time Argument

The discussion in Sec. II presented the physical ideas of the quark-parton model in momentum space. Now we will attempt to analyze the same physical picture in real space-time. First, we sketch the major issues before presenting details.

In the deep-inelastic process a quark parton is struck. It then propagates essentially freely and generates a cascade of partons. Eventually the partons of the cascade have finite momenta relative to some of the target partons left behind. These cascade partons are supposed to interact with the fragments of the target and carry away the anomalous charge from the struck parton.[5] Of course, the cascade partons can interact with the remnants of the target only if they can be generated in the same space-time vicinity as the target. Since the struck parton is presumed to travel near the speed of light, it is not clear *a priori* that this is possible. This is a very elementary point, but it is not in evidence in the momentum-space formulation of these ideas.

Let us be more precise. Consider the deep-inelastic process illustrated in Fig. 5. Choose the proton and virtual-photon momenta to be, respectively,

$$p_\mu = ((p^2 + m^2)^{1/2}, \vec{0}, p)$$

$$\approx (p + m^2/2p, \vec{0}, p) , \qquad (3.1)$$
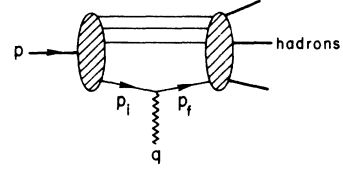
$$q_\mu \approx (\vec{Q}^2/2xp, \vec{Q}, 0) ,$$

FIG. 5. Deep-inelastic electroproduction in the parton model. p labels the target proton, q the virtual photon, p_i the parton before being struck, and p_f the parton after being struck.

where the proton has large momentum p in the z direction, vanishing transverse momentum, and $x = -q^2/2q \cdot p$. In such a frame one can consider the infinite-momentum wave function and constituents of the target proton. The momenta of the struck parton before and after its absorption of the virtual photon must then be

$$p_i \approx (xp + m^2/2xp, \vec{0}, xp) ,$$

$$p_f \approx p_i + q \qquad (3.2)$$

$$\approx (xp + (m^2 + \vec{Q}^2)/2xp, \vec{Q}, xp) ,$$

respectively. Dynamics in the infinite-momentum frame is clearer when expressed in terms of the variables H, $\vec{P}$, and η instead of E, $\vec{P}$, and p_z. Recall the definitions[7,8]

$$H = \frac{1}{\sqrt{2}} (E - p_z), \quad \vec{P} = \vec{P}, \quad \eta = \frac{1}{\sqrt{2}} (E + p_z) . \qquad (3.3)$$

These momenta are conjugate to the familiar space-time variables,

$$\tau = \frac{1}{\sqrt{2}} (t + z), \quad \vec{X} = \vec{X}, \quad \mathfrak{z} = \frac{1}{\sqrt{2}} (t - z), \qquad (3.4)$$

respectively. Then the parton momenta before and after the collision read

$$H_i \approx \frac{m^2}{2\sqrt{2}\, xp}, \quad \vec{P}_i \approx \vec{0}, \quad \eta_i \approx \sqrt{2}\, xp + \frac{m^2}{2\sqrt{2}\, xp},$$

$$\qquad (3.5)$$

$$H_f \approx \frac{m^2 + \vec{Q}^2}{2\sqrt{2}xp}, \quad \vec{P}_f \approx \vec{Q}, \quad \eta_f \approx \sqrt{2}\, xp + \frac{m^2 + \vec{Q}^2}{2\sqrt{2}xp} .$$

So, both the initial and final parton have $\eta \sim O(p)$ and differ significantly only in their transverse momenta. This is convenient, since boosts $\vec{B}$ which change transverse momenta but preserve η are especially simple in the infinite-momentum frame. They have a two-dimensional Galilean structure[7] and transform momenta according to the prescription

$$\vec{P} \xrightarrow{B} \vec{P} + \eta \vec{V} ,$$

$$\eta \rightarrow \eta , \qquad (3.6)$$

where $\vec{V}$ is the velocity of the transformation.

Thus, under such transformations $\vec{P}$ behaves as a two-dimensional Galilean momentum, η as a mass, and $\vec{V}$ as a two-dimensional velocity. Observe that the struck parton's momenta before and after absorption of the virtual photon are related via a Galilean boost of velocity

$$\vec{V} = \vec{Q}/\eta_i \; . \tag{3.7}$$

So, the evolution of the struck parton into its cascade can be first understood in a frame in which it has no transverse momentum. Then applying the boost defined by Eq. (3.7) produces the situation of interest here.

Cascades which are characterized by short-range correlations in momentum space have long been studied in the form of multiperipheral models. They are not traditionally studied in the infinite-momentum frame, although their dynamics is particularly transparent in such a formulation.[7,8] Two crucial properties of a cascade as depicted in Fig. 6 are:

(1) In each step of the cascade a certain average fraction α $(0 < \alpha < 1)$ of the η of the mth parton is carried off by the $(m+1)$st,

$$\eta_{m+1} \simeq \alpha \eta_m \; . \tag{3.8}$$

(2) Since the cascade is characterized by short-range correlations, the partons perform a random walk in the plane transverse to the infinite-momentum direction. So, after m steps of the cascade, the mean squared transverse distance between the first and mth parton is

$$\langle \vec{R}^2(m) \rangle \sim m \; . \tag{3.9}$$

With these facts it is easy to estimate the two most important quantities in our argument: the time (on the average) it takes for a cascade to generate a parton possessing a negligible fraction of the η_i of the struck parton, and the mean squared transverse position of that parton.

First consider the transverse position of the mth parton on a cascade. It follows from (1) that the average η of the mth parton is

$$\eta_m \sim \alpha^m \eta_i \; , \tag{3.10}$$

where η_i refers to the struck parton. Therefore,

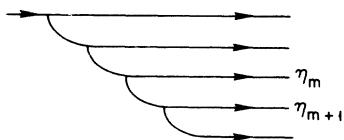$$\ln(\eta_m/\eta_i) \sim m \ln \alpha \; . \tag{3.11}$$

Substituting into Eq. (3.9),

FIG. 6. A multiperipheral cascade.

$$\langle \vec{R}^2(\eta_m) \rangle \sim \ln(\eta_m/\eta_i)/\ln\alpha \; . \tag{3.12}$$

Finally, the time τ_η it takes for a cascade to produce a parton having $\eta \ll \eta_i$ can be estimated on the basis of time dilation. The struck parton has a certain invariant amplitude for cascading into two others. If the cascade is then viewed in a reference frame moving with respect to the struck parton, the lifetime $\Delta\tau$ of the parton to cascade into two others is time dilated by a factor proportional to η_i,

$$\Delta\tau \sim \eta_i \; . \tag{3.13}$$

The time needed to produce a parton of Galilean mass η is then, approximately,

$$\tau_\eta \sim \sum_{\eta_i}^{\eta} \Delta\tau_i \sim \sum \frac{\Delta\tau_i}{\Delta\eta_i}\Delta\eta_i \sim \int_{\eta_i}^{\eta} \frac{d\tau}{d\eta} d\eta \; . \tag{3.14}$$

But from Eq. (3.8) the $\Delta\eta_i$ in each step of the cascade is

$$\Delta\eta_i \equiv \eta_i - \eta_{i+1} = (1-\alpha)\eta_i \; . \tag{3.15}$$

So, $\Delta\tau_i/\Delta\eta_i$ is independent of η_i, and the integral in Eq. (3.14) is just

$$\tau_\eta \sim \eta_i \; . \tag{3.16}$$

At this point we have sufficient understanding of a cascade of a parton with Galilean mass η_i and transverse momentum $\vec{P}_i = 0$ to consider again the cascade of the struck parton. After absorbing the virtual photon, the struck parton has transverse momentum $\vec{P}_f \cong \vec{Q}$. One of the partons in its cascade can interact with a parton remnant of the target only if their relative subenergy is small. From Eq. (3.6) we see that the transverse momentum of the cascade parton of Galilean mass η is

$$\vec{P} \approx \eta\vec{Q}/\eta_i \; . \tag{3.17}$$

In order to ensure that $\vec{P}$ be of order unity, one needs

$$\eta/\eta_i \sim 1/|\vec{Q}| \; . \tag{3.18}$$

This condition guarantees that the relevant subenergy can be small.

Now consider the transverse displacement $\vec{X}(\tau)$ of the struck parton a time τ after absorption of the virtual photon. From Eq. (3.7) and the Galilean character of transverse boosts, it is

$$\vec{X}(\tau) = (\text{Galilean velocity})(\text{time})$$
$$= (\vec{Q}/\eta_i)\tau \; . \tag{3.19}$$

Similarly, this transverse distance is a good estimate for the transverse distances of the fast $(\eta \approx \eta_i)$ products of the cascade. Consider $\vec{X}(\tau)$ itself and the transverse distance of the "wee" parton from $\vec{X}(\tau)$, $\vec{X}_\eta(\tau) - \vec{X}(\tau)$. If $\vec{X}_\eta(\tau)$ grows

with $\vec{Q}$, then the wee parton produced in the cascade cannot overlap in real space-time with the target at $\vec{X} \approx 0$ and presumably cannot interact with it (Fig. 7). But the wee parton is produced at a time

$$\tau_\eta \sim \eta_i ,$$

so

$$\vec{X}(\tau_\eta) \sim (\vec{Q}/\eta_i) \times \eta_i \sim \vec{Q} . \tag{3.20}$$

And the cascade performs a random walk from its center, so

$$\langle [\vec{X}_\eta(\tau_\eta) - \vec{X}(\tau_\eta)]^2 \rangle \sim \ln|\vec{Q}| , \tag{3.21}$$

for $\eta/\eta_i \sim 1/|\vec{Q}|$. Therefore, as $\vec{Q}$ becomes large the wee parton has a vanishingly small probability of being produced near $\vec{X} = 0$. This completes the argument.

It is interesting to discuss several aspects of this argument in more detail. First is the time-dilation argument which preceded Eq. (3.16). This type of argument is central to the parton model. In the description of $e + p \rightarrow e$ +anything, one views the proton in the infinite-momentum frame defined earlier, and argues that the internal interactions between the fast partons are slowed down by time dilation. Then one can argue that the virtual photon scatters incoherently off a quasifree parton. So, if one wants to build a picture of final states as has been suggested – where the final-state parton-parton interactions are of the same character as the parton-parton interactions that make up the hadron – then Eq. (3.16) follows quite generally.

Furthermore, in the argument we had to imagine that both the momentum and position of the struck parton were approximately described by suitable averages. Doing this can be subtle because of the constraints of the uncertainty principle. To be precise we can consider wave packets for the parton before and after it was struck by the virtual photon. Initially, the parton is confined in the transverse direction $\vec{X}$ to a diameter characteris-
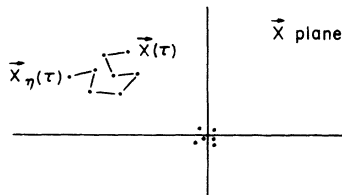

FIG. 7. The final-state parton configuration in the transverse plane. The partons near the origin are fragments of the target. The partons labeled $\vec{X}(\tau)$ through $\vec{X}_\eta(\tau)$ comprise the multiperipheral cascade of the struck parton.

tic of the hadron (1 F, say). In the longitudinal direction the wave function must be Lorentz contracted by a factor proportional to the parton's η. So, for illustrative purposes the initial wave function of the parton might be[9]

$$\psi_i(\tau, \vec{X}, \mathfrak{z}) \sim e^{i(H\tau + \eta \mathfrak{z} - \vec{P} \cdot \vec{X})}$$

$$\times \exp\left(-\frac{\eta^2}{2b^2} \mathfrak{z}^2\right) \exp\left(-\frac{1}{2a^2} \vec{X}^2\right) . \tag{3.22}$$

The momentum-space realization of ψ_i reads

$$\psi_i(\tau, \vec{P}', \eta') \sim e^{iH\tau} \exp\left[-i(\vec{P}' - \vec{P}) \cdot \frac{\vec{P}}{\eta} \tau\right]$$

$$\times \exp[-\tfrac{1}{2}b^2(1 - \eta'/\eta)^2]$$

$$\times \exp[-\tfrac{1}{2}a^2(\vec{P}' - \vec{P})^2] , \tag{3.23}$$

so the parton's transverse momentum and longitudinal fraction η'/η have finite uncertainties. After absorbing the virtual photon, the wave function of the struck parton is obtained from Eq. (3.22) by applying a Galilean boost $\vec{B}$ ($\vec{V} = \vec{Q}/\eta$), or by calculating the appropriate matrix element of the external probe $e^{i\vec{Q} \cdot \vec{X}}$,

$$\psi_f(\tau, \vec{X}, \mathfrak{z}) \sim e^{-i[H_{q+p} \tau + \eta \mathfrak{z} - (\vec{P} + \vec{Q}) \cdot \vec{X}]}$$

$$\times \exp\left(-\frac{1}{2b^2} \eta^2 \mathfrak{z}^2\right)$$

$$\times \exp\left[-\frac{1}{2a^2} \left(\vec{X} - \frac{(\vec{P} + \vec{Q})}{\eta} \tau\right)^2\right] , \tag{3.24}$$

where

$$H_{p+q} = \frac{(\vec{Q} + \vec{P})^2 + m^2}{2\eta} .$$

In particular, one notes that ψ_f is localized in the transverse plane about

$$\vec{X}(\tau) \approx \frac{(\vec{P} + \vec{Q})}{\eta} \tau ,$$

and the uncertainty in this relation is finite. So, the estimates used concerning Eq. (3.19) above suffice in a careful discussion based on reasonable wave functions. It is also clear that relations such as Eq. (3.19) do not depend on the fine details of ψ_i and ψ_f used for illustrative purposes here.[10]

A space-time picture can also be developed for electron-positron annihilation. The timelike photon dissociates into a parton-antiparton pair with momenta

$$p_1 = (p + m^2/2p, \vec{P}, 0),$$

$$p_2 = (p + m^2/2p, -\vec{P}, 0),$$

where $p = |\vec{P}|$. In the quark-parton picture of final states, these partons are then expected to initiate cascades. The wee partons in each cascade are then supposed to interact and neutralize the quark charges that were initially present in each cascade. To reduce this problem to the deep-inelastic case just studied, we boost the partons p_1 and p_2 along the z axis to large momentum. In this frame both partons have the same η, but they are moving apart with relative Galilean velocity of $2\vec{P}/\eta$ in the transverse plane. Now the earlier discussion of the important times and distances in multiperipheral cascades applies here, and again we conclude that the wee partons in each cascade do not overlap in real space-time.

This concludes our intuitive discussion. Although these arguments are not rigorously conclusive, they strongly suggest that the dynamics which holds the quark partons in must be of a newer and more interesting nature than conventional multiperipheral mechanisms. More discussion of this point will be given in Sec. V.

B. Energy Denominators and τ-Ordered Graphs

Another, and somewhat more conventional, way to understand the fact that multiperipheral mechanisms cannot generate the parton cascade illustrated in Fig. 3 is to study energy denominators for particular diagrams. Consider first the parton diagram shown in Fig. 8. In this process the struck parton cascades and generates a wee parton which interacts with a parton in the target. Interpret the diagram as a ϕ^3 graph, so it can illustrate the dynamics of the cascade but does not explicitly contain quantum numbers.

We want to know how the computation of this diagram would have to proceed in order that it satisfy the quark-parton physical picture. Clearly, the simplest diagram in this class, Fig. 9(a), contributes a term of order s^{-1}, while a graph with one additional rung [Fig. 9(b)] or more contributes terms of order s^{-2} to νW_2 $[s = (p+q)^2]$. However, summing over the rungs in the cascade of Fig. 8 *might* produce $\ln s$ factors which could sum to unity:

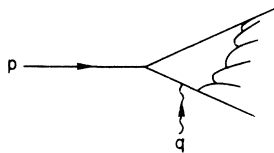$$\frac{1}{s^2} \sum \frac{1}{m!} (2 \ln s)^m = 1.$$

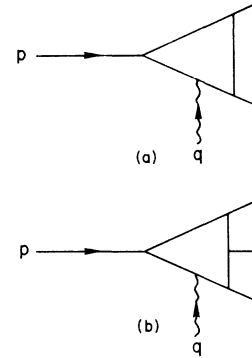FIG. 8. A ϕ^3 parton-model graph with a multiperipheral final-state interaction.

FIG. 9. (a) The simplest graph in the class of Fig. 8. (b) One additional rung inserted into graph (a).

Such behavior is found in multiperipheral models for on-shell *single* scattering processes.[7,8,11] If this occurred, the multiplicity of secondaries in the deep-inelastic process of Fig. 8 would grow ~$\ln s$, in agreement with the physical picture reviewed in Sec. II. Hence, in our graphical analyses we will search for $\ln s$ factors. If the calculations do not produce them, then short-range correlated multiperipheral mechanisms will not implement the ideas of Sec. II.

Let us redraw Fig. 8 and consider the process in the proton-photon center-of-mass frame with τ-ordered (old-fashioned perturbation-theory) graphs as in Fig. 10. Following Feynman,[12] we interpret the scattering event as composed of two parts. First, there are the wave functions of the projectile (photon, say) and target illustrated in Figs. 11(a) and 11(b). Second, there is an exchange of partons between these wave functions. We recall that the longitudinal momenta of the partons composing a hadron's wave function must sum to the hadron's total longitudinal momentum. Given these facts, which should be familiar,[12] we can understand Figs. 8 and 10 simply. First, since line i must be a member of both the right- and left-moving wave functions, it must carry a negligible longitudinal fraction, i.e., it is a wee parton.[12] However, if this parton is wee, the energy denominators in the photon wave function are of order p, its longitudinal momentum. Similarly,
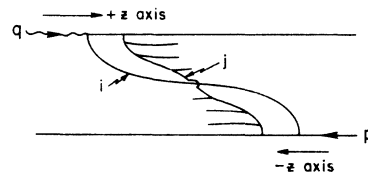

FIG. 10. Old-fashioned perturbation-theory graph representing the process of Fig. 8 in the photon-proton center-of-mass frame.
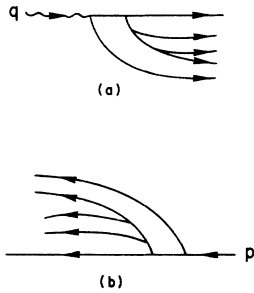
(a)

(b)

FIG. 11. (a) The photon wave function. (b) The proton wave function.

FIG. 12. A φ^3 parton-model graph with two multiperipheral chains in the initial state and a multiperipheral final-state interaction.

the energy denominators making up the proton wave function are of order p. This means that each time we insert an additional parton having a finite fraction of the longitudinal momentum of either the photon or the proton into the cascade (line j of Fig. 10), we pick up an additional energy denominator and a suppression by a factor p^{-1}. Hence, the cascade is strongly suppressed, cannot build up a Regge pole, and would not survive in the high-energy limit. Note that this argument did not even have to suppose that the photon was virtual, i.e., the cascade mechanism depicted in Fig. 10 does not even work for real photons. If, in addition, one allowed the photon to become virtual, then the argument becomes that much easier.

Let us turn now to a less trivial example. It is clear that one way to test the space-time argument is to let the target hadron be large (have a large area in the transverse plane). This idea leads us to consider the graph in Fig.12: The target hadron consists of two multiperipheral chains, a parton on one of those chains is struck, and that parton generates a cascade. Since wee partons in the target tend to spread out over large transverse distances $[\langle \vec{X}^2(\eta)\rangle \sim \ln\eta]$, this graph is a good can-
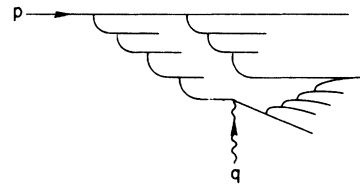
didate. The square of the amplitude Fig. 12 can be redrawn as the indicated discontinuity of a Feynman graph in Fig. 13. One recognizes that it is, in fact, the Mandelstam-cut diagram. Furthermore, if the photon is on shell, we know that this graph can be important at high energy and does show Regge-cut behavior in the variable s. Hence, this graph is much more interesting than Fig. 8. A detailed analysis of Fig. 13 will be given in Sec. IV and the appendixes.

It is worthwhile, however, to attempt to understand how the diagram works in simple terms. One way to do this is to study the graph in the lab frame with the virtual-photon momentum oriented along the z axis:

$$H_q = -Q^2/2\eta_q, \quad \vec{Q} = \vec{0}, \quad \eta_q,$$

$$H_p = \frac{m}{\sqrt{2}}, \quad \vec{P} = \vec{0}, \quad \eta = \frac{m}{\sqrt{2}},$$

(3.25)

$p \cdot q = \eta_q H_p \to \infty$, and $Q^2 \to \infty$ with $\omega^{-1} = Q^2/2p \cdot q$ fixed. However, before turning to the relatively complicated Mandelstam diagram, consider first the simple ladder graph in Fig. 14. The wave function for the virtual photon, shown in Fig. 15, has the formal expression[8,13]

$$|\psi_m\rangle = \frac{\lambda^{m-1}}{[(2\pi)^3]^m} \int \prod_{j=1}^{m} \frac{d^2K_j\,d\eta_j}{2\eta_j} (2\pi)^3\delta^2\left(\sum_{i=1}^{m} \vec{K}_i\right)\delta\left(\eta_q - \sum_{i=1}^{m} \eta_i\right)\prod_{i=1}^{m-1} [2\beta_i\Delta H_i]^{-1} (2\eta_m)\prod_{l=1}^{m} b^\dagger(\vec{K}_l, \eta_l)|0\rangle,$$ (3.26)
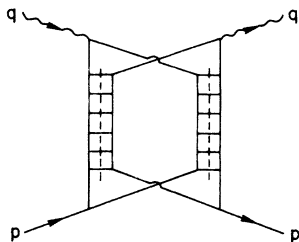

FIG. 13. The discontinuity giving the cross section for the process of Fig. 12. This is the Mandelstam discontinuity.
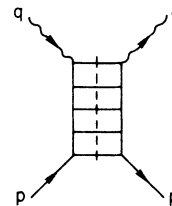

FIG. 14. The discontinuity of the simplest ladder model for deep-inelastic scattering.
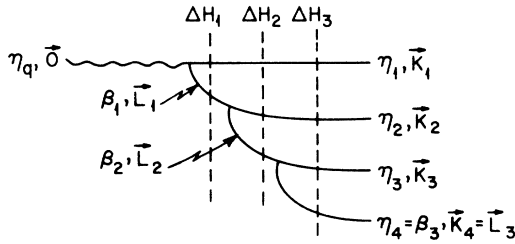
FIG. 15. A contribution to the photon wave function relevant to the calculation of the discontinuity of Fig. 14.

in mth order of the $\lambda\phi^3$ interaction. Each line in Fig. 15 is labeled with its longitudinal momentum (β's or η's) and transverse momentum ($\vec{L}$'s or $\vec{K}$'s), and the ΔH_i indicate infinite-momentum energy denominators. Consider the denominator factor,

$$2\beta_1 \Delta H_1 = 2\beta_1 \left[\frac{-Q^2}{2\eta_q} - \frac{\vec{K}_1^2 + m^2}{2\eta_1} - \frac{\vec{L}_1^2 + m^2}{2\beta_1} \right]. \quad (3.27)$$

Define a dimensionless, fractional variable x_1,

$$x_1 = \beta_1/\eta_q, \quad 1 - x_1 = \eta_1/\eta_q \ .$$

Then,

$$2\beta_1\Delta H_1 = -\left[Q^2 x_1 + \frac{1}{1-x_1}(\vec{L}_1^2 + m^2) \right]. \quad (3.28)$$

Similarly, the next factor $2\beta_2 \Delta H_2$ has the form

$$2\beta_2\Delta H_2 = -[Q^2 x_2 + \cdots],$$

where

$$x_2 = \beta_2/\eta_q < x_1 \ .$$

So, it is clear that if x_1 and x_2, say, were finite fractions, the wave function Eq. (3.26) would be suppressed by several powers of Q^2. Therefore, the important range of x_1 is very limited,

$$0 < x_1 \lesssim \mu^2/Q^2, \quad x_2 < x_1, \text{ etc.,} \quad (3.30)$$

where μ is some characteristic mass. This means that all the partons except $(\eta_1, \vec{K}_1)$ in the cascade carry a negligible fraction of the photon's η_q. In fact, the subenergy of parton $(\beta_1, \vec{L}_1)$ and the target becomes, roughly,

$$(x_1 q + p)^2 \approx 2 x_1 q \cdot p \approx 2\frac{p \cdot q}{Q^2}\mu^2 \approx \omega\mu^2, \quad (3.31)$$

where ω, the scaling variable (x^{-1}), is a finite number in the deep-inelastic region. Hence, on a rapidity plot the most likely positions of the partons in Fig. 14 would be as in Fig. 16. Also, since the subenergy in Eq. (3.31) is $\sim\omega$, the simple ladder graph must Reggeize in the variable ω. This is an elementary and well-known fact.[14] Of interest to us here are the facts that the internal lines
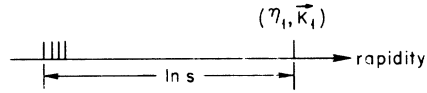

FIG. 16. Dominant configuration of partons in rapidity contributing to the process of Fig. 14. There is a rapidity gap $\sim \ln Q^2$ between the struck and next parton.

of Fig. 14 fall on the rapidity plot as in Fig. 16 — they are restricted to a finite subenergy of the target end — and the related fact that the graph generates $\ln^m\omega$, but not $\ln^m s$ terms.[15]

Now we can return to the Mandelstam graph. The τ-ordered graphs in the lab frame for the process shown in Fig. 12 are given in Fig. 17. From our analysis above we have that all the partons on the first chain have η values $\lesssim\omega$ except the parton $(\eta_1, \vec{K}_1)$. This means that all the energy denominators, such as for intermediate state 5 labeled in Fig. 17, are $\sim\omega^{-1}$. So, by the uncertainty principle, the total laboratory lifetime of the virtual-photon state before interacting with the target is $\sim\omega$. However, by time dilation, the amplitude per unit time for the second cascade to begin (vertex 2 in Fig. 17) is proportional to η_1^{-1}. And $\eta_1 \approx \eta_q$. Therefore, the amplitude that it occur in the available time interval $(\sim\omega)$ is $\sim\omega/\eta_q$. This amplitude goes to zero in the scaling region, which implies that this graph damps out as a power of the energy. To summarize, there just is not enough time available for the multiperipheral cascades to occur.

IV. PERTURBATION-THEORETIC REALIZATIONS

A. Motivation and Model

The simplest way in which we can try to realize the assumptions of the parton model and also study the effects of final-state interactions is in the context of renormalized perturbation theory. The only perturbation theories which are known to exhibit Bjorken scaling for both annihilation and deep-inelastic regions are superrenormalizable theories,[14] only one of which, namely the trilinear scalar the-
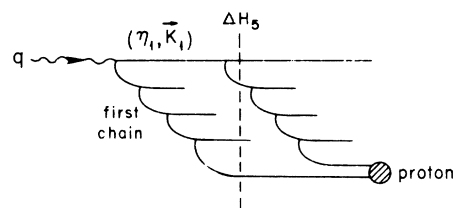

FIG. 17. Old-fashioned perturbation-theory graph of Fig. 15 in the laboratory frame.

ory, exists in four dimensions.[16] In renormaliza-
ble theories, even when we restrict ourselves to
those graphs which do not require renormalization,
we still fail to obtain scaling in the deep-inelastic
region.[17] Instead, there are logarithmic violations
of scaling, stemming from the fact that we are in
an exceptional momentum region.[18] In order to
retain scaling, which is fundamental to the parton
model, we resort to the artificial (noncovariant)
device of restricting the transverse-momentum
integrations. This artifice is due to Drell-Levy-
Yan.[19] We shall consider models in which a virtu-
al parton produced by the target hadron is struck
by the photon and then interacts with the "core"
(remnants of the target) by a multiperipheral cas-
cade in which many partons are produced. Fur-
thermore, we shall consider the case where the
parton is permitted to undergo bremsstrahlung
prior to being struck. The effect of a cascade be-
ing produced prior to the interaction will also be
considered.

We work in the frame where the photon momen-
tum is $q = (Q, -Q, \vec{0})$ and the initial hadron momen-
tum is $p = (m^2/\omega Q, \omega Q, \vec{0})$, where our components
are $(+, -, \vec{1})$. For a momentum k, $k_+ = k_0 + k_z$,
$k_- = k_0 - k_z$, and $\vec{k} = (k_x, k_y)$.[20]

(a)

(b)

FIG. 18. (a) Deep-inelastic electroproduction with
final-state interactions in ϕ^3 theory. (b) Discontinuity
giving cross section for (a).

B. The ϕ^3 and Drell-Lee Models

We first study a ϕ^3 model, which, although un-
physical, does scale.[14] For simplicity we consider
scalar photons for which the scaling law requires

$$\text{Disc} A(\nu, q^2) \sim W(\omega)/q^2 ,$$

where A is the amplitude whose discontinuity gives
the deep-inelastic cross section.

The first production mechanism considered is
that shown in Fig. 18(a), whose cross section
(neglecting interference) is given from the discon-
tinuity of Fig. 18(b). The graph corresponding to
Fig. 18(b) (without the discontinuity) is known to
behave like $(\ln s)/s^3$ at high energies[21] in the scat-
tering region $(q^2 = m^2)$. The absence of any $\ln^n s$
factors arising from the n ladder rungs is due to
the same mechanism that causes the absence of the
Amati-Fubini-Stanghellini (AFS) cut in planar
Feynman diagrams.[22] The contributions from the
two-particle intermediate states are canceled by
those from the multiparticle intermediate states.
Since we are taking an n-particle discontinuity,
it is necessary to check that the cancellations still
occur. Explicit calculation (Appendix A) reveals
that the discontinuity behaves like $1/s^3$. This was
to be expected since taking the n-particle discon-
tinuity still allows the two- and multiparticle dis-
continuities as before. It can also be seen that
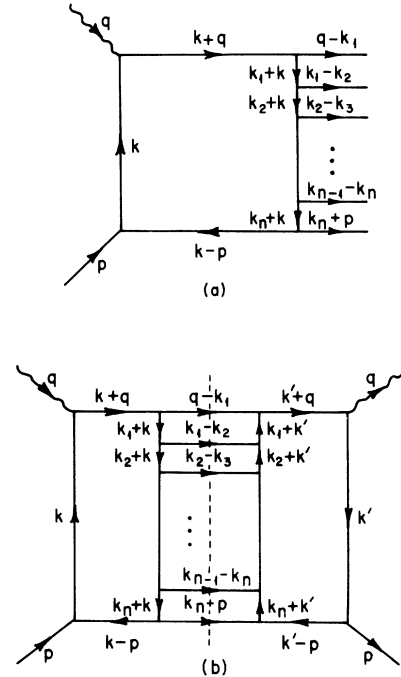the Cheng-Wu argument[23] for absence of the AFS

cut due to damping of the Reggeon in the external
mass variable is essentially unchanged by taking
the n-particle discontinuity.

In the deep-inelastic region, the graph (without
discontinuity) behaves like $(1/q^2)^3 F(\omega)$. The ex-
plicit calculation of Appendix A indicates that this
behavior obtains also for the n-particle discon-
tinuity of Fig. 18(b). Thus, we see that this pro-
duction mechanism does not contribute at high q^2,
since there are no $\ln^n q^2$ terms to sum to a power.
Thus, this is not a satisfactory final-state-inter-
action model.

A mention of the momentum distribution of the
final state will be of use for later discussions. It
is found that the leading power contribution comes
from the region where the first (leading) parton
has a + component of momentum $Q + O(1/Q)$ and a
– component of order $1/Q$, while the rest have a
– component proportional to Q and a + component
of order $1/Q$ and are thus fragments of the target.
The sum of all – components except the first must
also be of order $1/Q$.

Our second case of interest is that in which the
parton undergoes bremsstrahlung prior to being
struck, and then interacts with the core via a
multiperipheral cascade; see Fig. 19(a). The
cross section obtains from the discontinuity of the
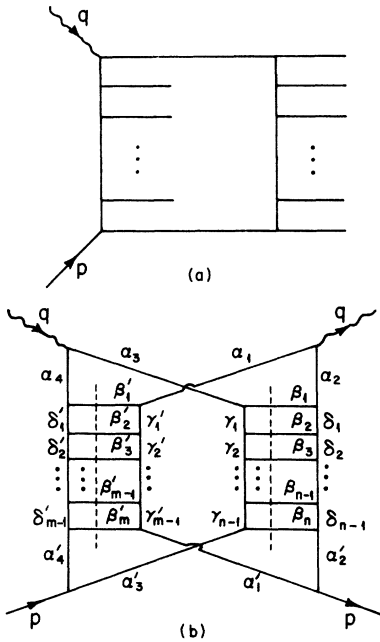Mandelstam graph,[24] Fig. 19(b), and the related

FIG. 19. (a) Deep-inelastic electroproduction with production before and after photon interaction in ϕ^3 theory. (b) Mandelstam discontinuity giving cross section for (a). Feynman parameters are those used in Appendix B.

"nondiagonal," interference graphs (see Appendix B). The Mandelstam graph behaves asymptotically in the scattering region like $(\ln^{m+n}s)/s^3$,[25] but, as shown in Appendix B, behaves like $(1/Q^2)^3\ln Q^2$ in the deep-inelastic region. This behavior is seen to be a bound on the interference graphs. The $\ln s$ factors become $\ln\omega$ factors in the large-ω region. The discontinuity behaves like $(1/Q^2)^3$. Such behavior has already been seen in the simple ladder graph[23] and is understood in terms of the behavior of the Regge residue functions for large external masses. That this behavior should extend to the Regge cut of the Mandelstam graph is therefore not surprising. Thus, the Mandelstam discontinuity is damped by 2 powers of Q^2 as was the simpler discontinuity. The distribution of particles in the final state can be seen to be the same as in the earlier case.

It is easy to see that this asymptotic vanishing of the final-state interaction as $(1/Q^2)^2$ times the scaling behavior and absence of $\ln^n Q^2$ factors which could sum to powers extends to the case of spin-one photons. It also occurs in Drell-Lee models,[26] where the charged parton is a fermion, but the interactions not involving the charged parton are trilinear scalar couplings. The composite nature of the initial hadron in their model is seen to be irrelevant to this conclusion.
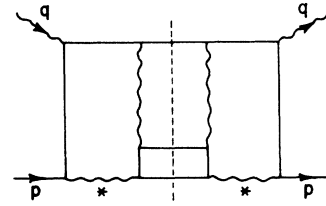

FIG. 20. Simple final-state interaction discontinuity in vector-gluon theory. * represents core.

C. The Fermion–Vector–Gluon Models

In this case the hadron and the struck parton are considered to be spin-$\frac{1}{2}$ fermions. The core left behind is treated as a neutral vector gluon despite the fact that it will carry (fractional) charge. The interaction is mediated by a neutral [SU(3) singlet] vector gluon.[27] The explicit introduction of a charge algebra is seen to give no essential complications to the calculations. The same results would obtain if the core was treated as a scalar or pseudoscalar.

Since vector exchange causes partons of large subenergy to scatter significantly, this interaction actually lies outside the strict bounds of the model of Sec. II. We consider it because in such a model the $(1/Q^2)^2$ factors which damped the asymptotic behavior in the previous subsection will be absent. One knows, for example, that a simple graph shown in Fig. 20 survives in the scaling region. Since a quark-parton model of this type would not normally scale,[27] we introduce a transverse momentum cutoff in the sense of Drell, Levy, and Yan.[19]

The simplest mechanism for final-state interactions, corresponding to Fig. 18 of the previous subsection, is given by the discontinuities of graphs, a typical one of which is shown in Fig. 21. For reasons of gauge invariance we are forced to include the graphs where vector gluons 1 and/or 2 interact before the photon.

The examination of this graph (see Appendix C) indicates that it yields asymptotic forms for W_1 and νW_2 which are independent of q^2 as desired.
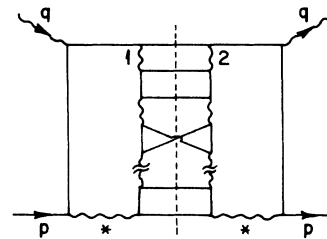

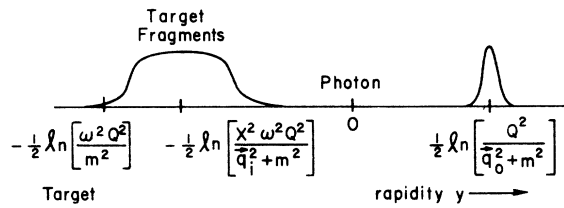FIG. 21. Final-state interaction discontinuity in fermion–vector-gluon theory.

FIG. 22. Final-state parton distribution in the fermion—vector-gluon model.

FIG. 24. More complicated "Mandelstam" type of discontinuity in the vector-gluon model.

The same is true for the other positions of gluons 1 and/or 2.

As in the scalar case, the leading parton has a + component of momentum $Q + O(1/Q)$ and a − component of order $1/Q$, while the rest have a − component proportional to Q and a + component of order $1/Q$ and are thus fragments of the target. The rapidity distribution of final partons is shown in Fig. 22. We note that there is a large rapidity gap, and hence large relative subenergy between the struck parton and the other produced partons, so that it is extremely unlikely that the struck parton can recombine with other partons. Thus, in a quark-parton model of this type we are forced to see a quark (parton) with fractional charge in the final state.

We have explicitly excluded vector gluons from the final state in this and later discontinuities. The reason for this is the following: If we did allow them in the final state we would, by gauge invariance, be forced to consider graphs where the gluons modify the photon vertices. Such modifications give nontrivial parton form factors in the deep-inelastic region and are thus not in the spirit of the parton model.[28] If, however, we included scalar and/or pseudoscalar particles, we could allow these to appear in the final state, since in a cutoff field theory, they give no vertex corrections in the Bjorken limit.[19]

If we did include such particles, graphs of the nature of Fig. 23 might naively be expected to give a resolution to the problem of fractional charge in
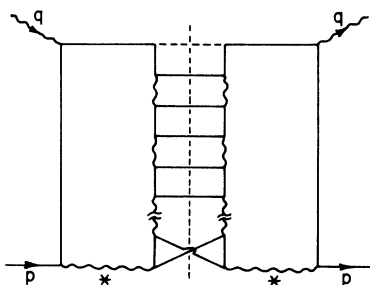
the final state, since a meson now replaces the leading parton in the final state. Such a graph, however, has fermion exchange with large subenergies in the cascade and is thus damped like $1/Q^2$.

Next we should consider the equivalent of the Mandelstam graph in ϕ^3. This is shown in Fig. 24. Here several parton-antiparton pairs are produced before a parton is struck by the photon and cascades. This parton is not, however, the initially produced parton. In this mechanism the final-state distribution is as before: a leading parton (the struck parton) which may be considered as a "photon fragment" and a number of target fragments (quarks or mesons if present). Thus the desired charge-exchange mechanism fails.

If we included scalar (pseudoscalar) mesons we would have a second form of Mandelstam graph, namely, that in which the produced parton emits mesons by bremsstrahlung before being struck by the photon, and then cascades. This is illustrated in Fig. 25. The final-state distribution is the same as before, and again the contribution scales.

Therefore, in all cases studied, the rapidity gap between the struck parton and core is not filled by the cascade. In addition, the average multiplicities are finite, since the sum of the + components of momenta of particles in the target fragmentation region is always of order $1/Q$. So, none of these perturbation-theoretic parton models is a realization of the Bjorken-Feynman model.[1−4]

FIG. 23. Final-state interaction modified to include scalar (pseudoscalar) meson (broken line) in the final state.

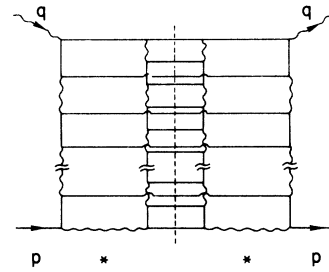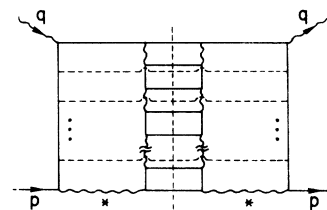FIG. 25. Mandelstam discontinuity modified by inclusion of scalar (pseudoscalar) mesons.

D. e^+e^- Single Photon Annihilation

In the ϕ^3 case, we consider first the process where the timelike photon from the e^+e^- annihilation "decays" into a parton-antiparton pair. The pair interacts via a multiperipheral-type cascade producing a multiparticle final state. This process is illustrated in Fig. 26(a). Its cross section is given by the discontinuity of Fig. 26(b). We first consider the case for scalar photons, where we find that, except for the two-rung case which behaves like Q^{-4}, the discontinuities behave asymptotically like Q^{-6} (with no powers of $\ln Q^2$) (see Appendix D), in contrast with the constant required for scaling.

For later reference, we note that except for the initial parton-antiparton pair, one of which has $+$ momentum of order Q and $-$ momentum of order $1/Q$, while the other has $-$ momentum of order Q and $+$ momentum of order $1/Q$, the rest are produced in a bunch. The character of such a bunch is that all the plus momenta behave like a fixed power of Q, Q^α say $(-1 \leq \alpha \leq 1)$, while the minus momenta behave like $Q^{-\alpha}$. The total momentum will then also have $(+,-)$ components like $(Q^{+\alpha}, Q^{-\alpha})$.

We will also consider a second mechanism where one of the produced particles undergoes bremsstrahlung (see Fig. 27). This time the discontinuity W scales, but the isolated parton has most of either the $+$ or $-$ component of momentum $(\simeq Q)$, while the other particles share the other large-

(a)

(b)

FIG. 27. (a) Single-photon e^+e^- annihilation with fragmentation of one parton in ϕ^3 theory. (b) Discontinuity yielding cross section for (a).

momentum component. This gives a large rapidity gap between the isolated parton and the bunch, so that charge exchange is impossible. The multiplicity is finite.

The replacement of the external lines by vector photons leaves the results essentially unchanged (except perhaps in the low-order cases), as does the introduction of a single fermion loop as in the Drell-Lee models.

For the cutoff fermion–vector-gluon model our cross section for the cascade process is given by the discontinuity of graphs such as that of Fig. 28. Disallowing the lowest-order graph which is associated with the nontrivial form factors of such a theory, we find a scaling result. The final-state distribution is the same as found for the ϕ^3 case. Thus we find bunching and finite multiplicities. The three forms of distribution are illustrated in Fig. 29. The first case [Fig. 29(a)] shows the production of a bunch of partons with $+$ momenta of order Q^α, $-$ momenta of order $Q^{-\alpha}$ $(-1 < \alpha < 1)$. The second and third are the fragmentation $\alpha = \pm 1$ cases. As we see, although the
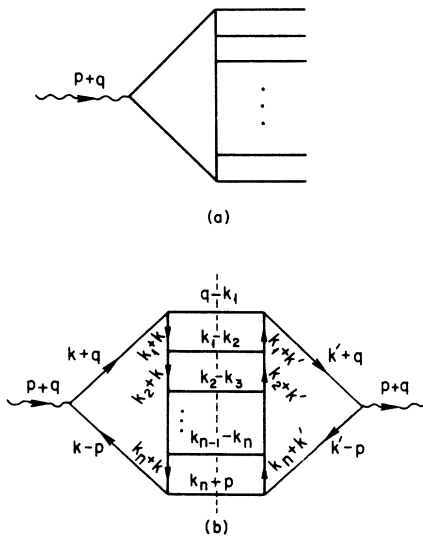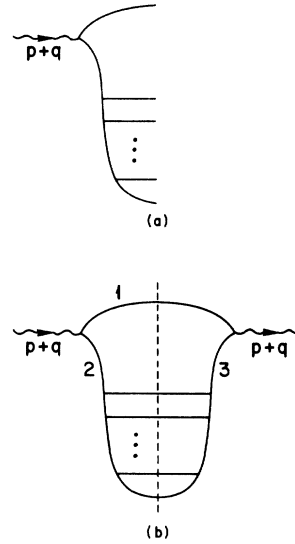

(a)

(b)

FIG. 26. (a) Single-photon e^+e^- annihilation with final-state interaction in ϕ^3 theory. (b) Discontinuity yielding the cross section for (a).
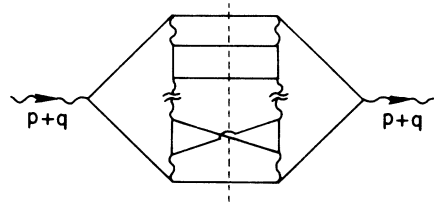

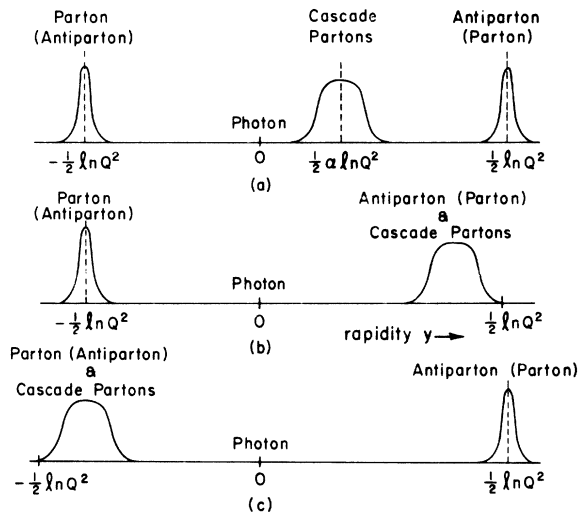FIG. 28. e^+e^--annihilation final-state discontinuity in fermion–vector-gluon theory.

FIG. 29. Final-state distributions in e^+e^- annihilation.
(a) Bunching in central region. (b), (c) Parton fragmentation.

FIG. 30. (a) Parton-fragmentation discontinuity in vector-gluon theory of e^+e^- annihilation. (b) Crossed graph required for gauge invariance.

one-particle spectrum is going to be a relatively flat curve from $y = -\frac{1}{2}\ln Q^2$ to $y = \frac{1}{2}\ln Q^2$, the correlation functions will show this strongly correlated bunching. Since fermion exchange between bunches would lead to damping of the amplitude by a power of Q [$(Q^2)^{-1\pm\alpha}$ to be exact], a charge-exchange mechanism which would require one or two such exchanges is damped by 1 power of Q^2. Thus for large Q^2 we cannot neutralize the quark charge, and quarks would be seen in the final state.

The equivalents of Fig. 27, viz., Fig. 30, which are required by gauge invariance, populate only the fragmentation regions as in the ϕ^3 case, and thus do not change the above argument.

As in the deep-inelastic region, we have explicitly avoided vector-gluon production and its accompanying difficulties.

V. CONCLUSIONS AND DISCUSSION

We have examined the feasibility of a cascade mechanism for final-state interactions for deep-inelastic scattering and one-photon e^+e^- annihilation in the context of the quark-parton model. The purpose of this was to see whether such interactions could neutralize the quark charge and prevent particles with quark quantum numbers from being observed in the final state. We have examined this both in an intuitive space-time argument and in models based on relativistic perturbation theory. The results in both arguments are the same. The cascade mechanism fails, and quarks are produced in the final state.
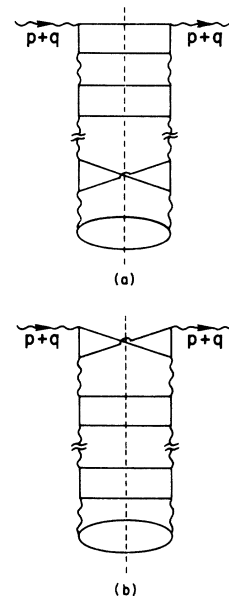
It can be seen that modifications to our scheme,

in which some of the partons are produced prior to the cascade which yields the struck parton, do not affect the result. However, in the perturbation-theory models one might suspect that if the parton propagator were modified to prevent large invariant parton masses, then the AFS result with final states evenly distributed in the rapidity plot would follow. But the space-time argument, being valid for invariant parton masses near the mass shell, shows that this is incorrect, and at best the same conclusions hold as for normal propagators.

These models, of course, are artificial: Firstly, because ϕ^3 is not a physical theory, and the cutoff procedure is noncovariant and nonunitary; and secondly, our choice of Feynman diagrams must be suitably restricted in order to obtain scaling parton theories. The intuitive arguments are at best plausibility arguments based on a naive physical picture. Thus, we must consider our results as suggestive but not conclusive.

Our spectrum of final-state partons in the deep-inelastic case consists of a leading parton traveling in the direction of the incoming photon and a finite number of target fragments. Absent is any vestige of the flat rapidity distribution suggested by the model described in Sec. II. For the annihilation process our one-particle spectrum will be smooth, but the two-and-more-particle correlations will indicate that, with the exception of the initially produced parton-antiparton pair, the rest of the partons produced will be bunched.

Our calculations also shed doubt on several ideas and models in the literature. Models have been proposed for the electromagnetic form factors of hadrons,[29] deep-inelastic scattering,[30] and electron-positron collisions.[31] These models insert strong-interaction amplitudes into an electromagnetic process. For example, Ref. 29 considers a model of the pion form factor based on the diagram in Fig. 31. Here the strong final-state interaction is represented by an *on-shell* Veneziano amplitude, i.e., the dependence the amplitude might have on the legs 1 and 2 is ignored. The reason for doing this is simply that a reliable prescription for taking a dual amplitude off the mass shell is not known. However, one does know how to extend simple ladder graphs off shell. In fact, the composite nature of perturbation-theoretic Regge poles leads to residue functions which fall to zero quickly as an external leg goes off shell.[23] Our conclusion that the simple ladder-graph model (Fig. 26) for the annihilation channel does not satisfy the Bjorken-Feynman model can be traced, in fact, to the damping provided by the residue functions. In view of the fishnet[32] interpretation of the Veneziano model, it is hard to believe that the residue functions of a complete dual model would be less convergent than those of ladder graphs. In any event, the models of Refs. 29–31 are not supported by explicit graphical calculations.

Finally, we should ask ourselves what new features parton-parton interactions must have in order that the Bjorken-Feynman picture might work. In addition to producing forces of short range in momentum space, our multiperipheral and perturbation-theory graphs generate forces which also have only short range in configuration space. If we let the interaction extend over long distances in real space (a harmonic potential, say), then quark partons could probably be confined to the nucleon. In addition, our space-time criticism, which assumes that the struck parton propagates essentially freely, would not apply to such models. Quark-parton models with long-range forces have been discussed by Johnson.[33] He has shown that such schemes have many good features and, surprisingly, are not necessarily in contradiction with the sacred tenets of field the-
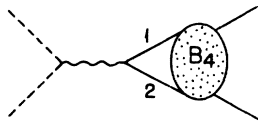

FIG. 31. Model of e^+e^- annihilation considered in Ref. 29. B_4 is the relevant on-shell Veneziano cross section.

ory. It remains to be seen if such models produce a physical picture of deep-inelastic final states in agreement with Bjorken-Feynman ideas. We hope to answer this question in the near future.

APPENDIX A: SINGLE CASCADE MODEL FOR FINAL-STATE INTERACTIONS IN ϕ^3 THEORY

We consider the behavior of the discontinuity of Fig. 18(b) evaluated in the deep-inelastic region $(q_+ = Q,\ q_- = -Q,\ \vec{q} = \vec{0},\ p_+ = m^2/\omega Q,\ p_- = \omega Q,\ \vec{p} = \vec{0}$, with $Q \to +\infty$, ω fixed). For simplicity we consider the photons as scalars.

Since the asymptotic behavior of the graph itself is known to be $\sim(1/Q^2)^3$, [21,23] we will neglect all terms which decrease faster by a power than this. In fact, for our calculation, we shall concentrate solely on the k integration, and thus pick only those contributions which fall no faster than $1/Q^2$, since we will obtain a second factor of $1/Q^2$ from the k' integration and a third from the ladder rungs.[34] Maximal use is made of previous momentum-space calculations, from which it is gleaned that factors of $\ln s$ (and hence $\ln Q^2$) are obtained only when our (+) and (−) components of the ladder loop momenta are strongly ordered[34]:

$$k_{i+} \gg k_{i+1+}; \quad k_{i-} \gg k_{i+1-}, \tag{A1a}$$

or

$$k_+ + k_{i+} \gg k_+ + k_{i+1+};$$
$$k_- + k_{i-} \gg k_- + k_{i+1-}. \tag{A1b}$$

For each of the ladder rungs we have a factor

$$\theta(k_i^0 - k_{i+1}^0)\delta((k_i - k_{i+1})^2 - m^2). \tag{A2}$$

These factors order the momenta k_i, viz.,

$$-\omega Q < k_{n-} < k_{n-1-} < \cdots < k_{2-} < k_{1-} < -Q, \tag{A3a}$$

$$-\frac{m^2}{\omega Q} < k_{n+} < k_{n-1+} < \cdots < k_{2+} < k_{1+} < Q. \tag{A3b}$$

Now we must examine the poles in the variable k_+.

The denominator $k^2 - m^2 + i\epsilon$ gives rise to a pole at

$$k_+ = \frac{\vec{k}^2 + m^2 - i\epsilon}{k_-} , \qquad (A4)$$

which is in the upper-half k_+ plane for $k_- < 0$, and in the lower half plane for $k_- > 0$.

The denominator $(k+q)^2 - m^2 + i\epsilon$ gives rise to a pole at

$$k_+ = -Q + \frac{\vec{k}^2 + m^2 - i\epsilon}{k_- - Q} , \qquad (A5)$$

which is in the upper half plane for $k_- < Q$, and in the lower half plane for $k_- > Q$.

The denominator $(k-p)^2 - m^2 + i\epsilon$ gives rise to a pole at

$$k_+ = \frac{m^2}{\omega Q} + \frac{\vec{k}^2 + m^2 - i\epsilon}{k_- - \omega Q} , \qquad (A6)$$

which is in the upper half plane for $k_- < \omega Q$, and in the lower half plane for $k_- > \omega Q$.

The denominator $(k+k_j)^2 - m^2 + i\epsilon$ gives rise to a pole at

$$k_+ = -k_{j+} + \frac{(\vec{k}_j + \vec{k})^2 + m^2 - i\epsilon}{k_{j-} + k_-} , \qquad (A7)$$

which is in the upper half plane for $k_- < -k_{j-}$, and in the lower half plane for $k_- > -k_{j-}$, where $Q < -k_{j-} < \omega Q$.

Thus, we see that for $k_- < 0$ all poles are in the upper half k_+ plane, while for $k_- > \omega Q$ all poles are in the lower half k_+ plane. Hence, the only contribution to the k_- integral comes from the range

$$0 < k_- < \omega Q . \qquad (A8)$$

We choose to close the k_+ contour in the lower half plane, hence picking up the residues of poles (A4), (A5), and (A7), but not (A6).

Before proceeding we introduce the definitions of $\sim$ and $\simeq$ as used in the following:

$$a \sim b \text{ means } \lim_{Q \to \infty} a/b = \text{const} , \qquad (A9)$$

$$a \simeq b \text{ means } \lim_{Q \to \infty} a/b = 1. \qquad (A10)$$

Evaluated at the pole in (A4) our denominators become

$$(k+q)^2 - m^2 + i\epsilon = Q(k_- - Q) + (k_- - Q)\left(\frac{\vec{k}^2 + m^2 - i\epsilon}{k_-}\right) - \vec{k}^2 - m^2 + i\epsilon , \qquad (A11)$$

$$(k-p)^2 - m^2 + i\epsilon = -\frac{m^2}{\omega Q}(k_- - \omega Q) + (k_- - \omega Q)\left(\frac{\vec{k}^2 + m^2 - i\epsilon}{k_-}\right) - \vec{k}^2 - m^2 + i\epsilon, \qquad (A12)$$

$$(k_i + k)^2 - m^2 + i\epsilon = k_{i+}(k_- + k_{i-}) + (k_- + k_{i-})\left(\frac{\vec{k}^2 + m^2 - i\epsilon}{k_-}\right) - (\vec{k} + \vec{k}_i)^2 - m^2 + i\epsilon , \qquad (A13)$$

while the measure for the k_- integration is dk_-/k_-, with $0 < k_- < \omega Q$. Now let us consider the behavior of this integral for various regions of the k_- integration (transverse components assumed finite).

Case 1: $k_- \sim 1/Q$. (A11) and (A12) give a contribution $\sim Q^{-4}$.

Case 2: $k_- \sim 1$. (A11) and (A12) give a contribution $\sim Q^{-3}$.

Case 3: $k_- \sim Q$. Points with $k_- \simeq Q$ can be avoided by deforming the k_- integration contour. We obtain a contribution $\sim Q^{-2}$ from (A11) and (A12). From (A13) we see that we must require either $k_{i+} \sim 1/Q$ or $k_{i-} \simeq -k_-$. Unless $k_{i-} \simeq -\omega Q$ then the point $k_- \simeq -k_{i-}$ can be avoided (by $\sim Q$) by deformation of the contour. But for $k_- \simeq -k_{i-} \simeq \omega Q$, the measure dk_-/k_- damps this contribution. So all $k_{i+} \sim 1/Q$; there is no strong ordering nor powers of $\ln Q^2$.

Next we consider the pole (A5), which contributes for $Q < k_- < \omega Q$. The propagator denominators in this case are

$$k^2 - m^2 + i\epsilon = -Qk_- + k_-\left(\frac{\vec{k}^2 + m^2 - i\epsilon}{k_- - Q}\right) - \vec{k}^2 - m^2 + i\epsilon , \qquad (A14)$$

$$(k-p)^2 - m^2 + i\epsilon = -\left(Q + \frac{m^2}{\omega Q}\right)(k_- - \omega Q) + (k_- - \omega Q)\left(\frac{\vec{k}^2 + m^2 - i\epsilon}{k_- - Q}\right) - \vec{k}^2 - m^2 + i\epsilon , \qquad (A15)$$

$$(k_i + k)^2 - m^2 + i\epsilon = (k_{i+} - Q)(k_{i-} + k_-) + (k_{i-} + k_-)\left(\frac{\vec{k}^2 + m^2 - i\epsilon}{k_- - Q}\right) - (\vec{k}_i + \vec{k})^2 - m^2 + i\epsilon , \qquad (A16)$$

while the measure for the k_- integration is $dk_-/(k_- - Q)$.

We now consider the behavior of the various regions of k_- integration as follows.

Case 1: $k_- \sim Q$. The contribution of (A14) and (A15) alone is $\sim Q^{-4}$ unless $k_- \simeq Q$ or $k_- \simeq \omega Q$.

Case 2: $k_- \simeq \omega Q$. If the denominators (A14) and (A15) are not to produce a contribution which damps faster than $\sim 1/Q^2$, then we must require $k_- = \omega Q + O(1/Q)$. But this requires that the measure $dk_-/(k_- - Q)$ $\sim 1/Q^2$, and so the contribution is still damped.

Case 3: $k_- \simeq Q$. That (A14) and (A15) do not produce a damped contribution requires

$$- Qk_- + k_-\left(\frac{\vec{k}^2 + m^2 - i\epsilon}{k_- - Q}\right) \sim Q . \tag{A16}$$

This has a solution of the form $k_- = Q + O(1/Q)$. Hence,

$$Q - \left(\frac{\vec{k}^2 + m^2 - i\epsilon}{k_- - Q}\right) \sim 1 . \tag{A17}$$

Thus,

$$k_- = Q + \frac{\vec{k}^2 + m^2 - i\epsilon}{Q} + O(1/Q^2) . \tag{A18}$$

This condition makes both (A14) and (A15) each $\sim Q$. But we may avoid this point by a contour of the form of Fig. 32, on which the contribution of (A14) and (A15) is $\sim Q^{-4}$.

Finally, we consider the contribution of poles of the form of (A7). For a typical pole of this class, the denominators are

$$k^2 - m^2 + i\epsilon = -k_{j+}k_- + k_-\left(\frac{(\vec{k}_j + \vec{k})^2 + m^2 - i\epsilon}{k_{j-} + k_-}\right) - \vec{k}^2 - m^2 + i\epsilon , \tag{A19}$$

$$(k+q)^2 - m^2 + i\epsilon = (Q - k_{j+})(k_- - Q) + (k_- - Q)\left(\frac{(\vec{k}_j + \vec{k})^2 + m^2 - i\epsilon}{k_{j-} + k_-}\right) - \vec{k}^2 - m^2 + i\epsilon , \tag{A20}$$

$$(k-p)^2 - m^2 + i\epsilon = -\left(k_{j+} + \frac{m^2}{\omega Q}\right)(k_- - \omega Q) + (k_- - \omega Q)\left(\frac{(\vec{k}_j + \vec{k})^2 + m^2 - i\epsilon}{k_{j-} + k_-}\right) - \vec{k}^2 - m^2 + i\epsilon , \tag{A21}$$

$$(k_i + k)^2 - m^2 + i\epsilon = (k_{i+} - k_{j+})(k_{i-} + k_-) + (k_{i-} + k_-)\left(\frac{(\vec{k}_j + \vec{k})^2 + m^2 - i\epsilon}{k_{j-} + k_-}\right) - (\vec{k}_i + \vec{k})^2 - m^2 + i\epsilon , \tag{A22}$$

while the measure is $dk_-/(k_- + k_{j-})$. The integration range is $Q < -k_{j-} < k_- < \omega Q$.

Case 1: $k_- \sim Q$ *(required by integration limits).* We exclude for the present $k_- \simeq -k_{j-}$. This contribution decreases faster than Q^{-2} unless $k_{j+} \sim 1/Q$. Then the contribution of (A19), (A20), and (A21) is $\sim Q^{-2}$. For the total denominator contribution to be of this order requires $k_{i+} \sim 1/Q$ or $k_{i-} \simeq -k_-$. This latter point can be avoided unless $k_{i-} \simeq -\omega Q$, but then the measure $dk_-/(k_- + k_{j-})$ damps this contribution, since $k_- \not\simeq -k_{j-}$. So we must have all $k_{i+} \sim 1/Q$, and hence there is no strong ordering of the k_{i+}'s and hence no powers of $\ln Q^2$.

Case 2: $k_- \simeq -k_{j-}$. First we shall exclude the case $-k_{j-} \simeq Q$. Assuming $k_- + k_{j-} \sim Q^\alpha$ ($\alpha < 1$), we find that denominators (A19), (A20), and (A21) give at best a contribution $\sim Q^{-4+2\alpha}$, which is asymptotically damped relative to Q^{-2}.

Case 3: $k_- \simeq -k_{j-} \simeq Q$. Since the best behavior (least damped) will come when $k_- + k_{j-} \sim k_- - Q \sim Q^\alpha$ ($\alpha < 1$), say, we restrict our consideration to this case. The best behavior (which occurs for $k_{j+} \sim 1/Q$) is that the denominators (A19), (A20), and (A21) give a contribution $Q^{-3+\alpha}$, which is damped

relative to Q^{-2}. Similar results hold for $k_- \simeq -k_{j-} \simeq \omega Q$.

Case 4: Special case. We note here that one might expect better asymptotic behavior for

$$k_{j+} \simeq \frac{(\vec{k}_j + \vec{k})^2 + m^2 - i\epsilon}{k_- + k_{j-}}, \tag{A23}$$

so that

$$k_- \simeq -k_{j-} + \frac{(\vec{k}_j + \vec{k})^2 + m^2 - i\epsilon}{k_{j+}} . \tag{A24}$$

Subcase 1: $k_{j+} \sim 1/Q$. Then $k_- = -k_{j-} + O(Q)$. This point can be avoided by deforming the k_- contour by a distance $\sim Q$. On such a contour we are back to Case 1.
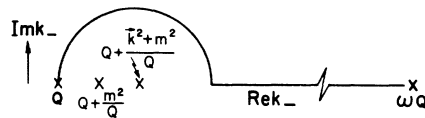

FIG. 32. Contour used to avoid point $k_- = Q + (\vec{k}^2 + m^2)/Q + O(1/Q^2)$ in Appendix A.

Subcase 2: $k_{j+} \sim Q^{\alpha}$ $(-1 < \alpha < 1)$. Then $k_- = -k_{j-} + O(Q^{-\alpha})$ and contour deformation permits us to avoid this point by $\sim Q^{-\alpha}$, thus returning us to Case 2.

Subcase 3: $k_{j+} \sim Q$. Put $k_{j+} \simeq xQ$. Then $0 < x \leqslant 1$ from (A3b). Hence, we may avoid this point by at least m^2/Q and thus obtain a contribution $\sim Q^{-6}$ from the denominators (A19), (A20), and (A21) (except for $k_- \simeq Q$ or $k_- \simeq \omega Q$, when they give a contribution $\sim Q^{-4}$).

Hence, we have found that our asymptotic behavior of the discontinuity of Fig. 18(b) is $\sim (1/Q^2)^3$ with no factors of $\ln Q^2$. All the momenta k_i have $k_{i+} \sim 1/Q$. Thus, all the final-state particles except the leading parton have plus momenta $\sim 1/Q$ and minus momenta $\sim Q$. The sum of all their plus components is also $\sim 1/Q$. The cross section for $(n+1)$-particle production will have a factor $1/n!$ from the phase-space integrations.[35] This factor causes the average multiplicity to be a constant (independent of Q^2) for large Q and fixed ω.

APPENDIX B: THE MANDELSTAM GRAPH

The Mandelstam graph [Fig. 19(b)] behaves like $\sim (1/s)^3 (\ln s)^{m+n}$ as $s \to \infty$ in the scattering region $(q^2 = m^2)$.[21,24,25] Thus, we expect that if the $(\ln s)^{m+n}$ becomes a $(\ln Q^2)^{m+n}$ in the deep-inelastic discontinuity, then this factor would show up in the graph itself in this region. Hence, for simplicity, we restrict ourselves to the investigation of the graph itself in the deep-inelastic region.

We use the Feynman-parameter techniques of Ref. 21. The coefficient of s in the denominator is of the form[25]

$$g = C(\alpha)xy + R(\alpha) , \tag{B1}$$

where

$$x = \alpha_1\alpha_3 - \alpha_2\alpha_4 , \tag{B2}$$

$$y = \alpha_1'\alpha_3' - \alpha_2'\alpha_4' . \tag{B3}$$

After evaluating the pinch (which would exist in the scattering region) at

$$x \sim \beta ; \quad y \sim \beta , \tag{B4}$$

we would find that $R(\alpha)$ vanishes if we put one of $\beta_1, \ldots, \beta_{n-1} = 0$ and one of $\beta_1', \ldots, \beta_{m-1}' = 0$. It is found that putting either $(\alpha_1, \alpha_4) = 0$ or $(\alpha_2, \alpha_3) = 0$ and $(\alpha_1', \alpha_4') = 0$ or $(\alpha_2', \alpha_3') = 0$ also causes $R(\alpha)$ to vanish after evaluating the pinch. Then, for a typical pair (β, β'), we write

$$\beta = \rho\bar{\beta}; \quad \beta' = \rho\bar{\beta}' ;$$

$$d\beta d\beta' = \rho \, d\rho d\bar{\beta}d\bar{\beta}' \, \delta(\bar{\beta} + \bar{\beta}' - 1). \tag{B5}$$

We can rewrite the linearized form of g, viz., $\bar{g}$, as

$$\bar{g} = \bar{C}xy + \rho_1\rho_2 \cdots \rho_{m+n+1} \bar{f}(\alpha) . \tag{B6}$$

Now, for the deep-inelastic case our coefficient of Q^2 can be written as

$$-h = \alpha_4 A + \beta_1' B + \alpha_1 C . \tag{B7}$$

So we may scale α_4, β_1', and α_1, viz.,

$$\alpha_4 = \sigma\bar{\alpha}_4; \quad \beta_1' = \sigma\bar{\beta}_1'; \quad \alpha_1 = \sigma\bar{\alpha}_1;$$

$$d\alpha_4 d\beta_1' d\alpha_1 = \sigma^2 d\sigma d\bar{\alpha}_4 d\bar{\beta}_1' d\bar{\alpha}_1 \delta(\bar{\alpha}_4 + \bar{\beta}_1' + \bar{\alpha}_1 - 1). \tag{B8}$$

Similarly, we may scale α_2, β_1, and α_3 by σ'. h then becomes

$$h = \sigma\sigma' h'(\alpha). \tag{B9}$$

Similarly,

$$g = \sigma\sigma' g'(\alpha). \tag{B10}$$

Since Q^2 and $s \to \infty$ together, with

$$s = (\omega - 1)Q^2 ,$$

then we need to find the zeros of

$$(\omega - 1)g - h$$

in order to determine the asymptotic behavior of the amplitude.

We see that no longer do we have a pinching zero, but merely the endpoint zeros at $\sigma = 0$ and $\sigma' = 0$. Hence, the asymptotic behavior in Q^2 is $\sim (1/Q^2)^3 \ln Q^2$. The discontinuity is then $\sim (1/Q^2)^3$.

This asymptotic behavior of the discontinuity is verified by explicit calculation, not presented here because it is extremely lengthy and is rather similar to that of Appendix A. The explicit calculation indicates that the same spectrum of final states is obtained as for the case in Appendix A.

Now let us consider the "interference" discontinuities referred to in Sec. IV B. If we denote the amplitude for the production process, Fig. 19(a), by $A(1, 2, \ldots, m; m+1, \ldots, m+n)$ then the Mandelstam discontinuity is proportional to

$$\int |A(1, 2, \ldots, m; m+1, \ldots, m+n)|^2 \, d\varphi_{m+n} , \tag{B11}$$

where φ_{m+n} is $(m+n)$-particle phase space. A typical interference contribution is then proportional to

$$\int A^*(1, 2, \ldots, m; m+1, \ldots, m+n)A(i_1, i_2, \ldots, i_m; i_{m+1}, \ldots, i_{m+n}) \, d\varphi_{m+n} , \tag{B12}$$

where $(i_1, \ldots, i_{m+n})$ is some permutation of $(1, \ldots, m+n)$. This serves to define what we mean by an "interference" graph.

We note immediately that using Schwarz's inequality gives

$$\left| \int A^*(1, 2, \ldots, m; m+1, \ldots, m+n) A(i_1, i_2, \ldots, i_m; i_{m+1}, \ldots, i_{m+n}) d\varphi_{m+n} \right|$$

$$\leq \int |A(1, 2, \ldots, m; m+1, \ldots, m+n)|^2 d\varphi_{m+n} .$$

Thus the asymptotic behavior of such discontinuities is bounded by that of the Mandelstam graph, and hence, in the deep-inelastic case, by the $(Q^2)^{-3}$ result. A refinement of this argument can be used to eliminate the possibility of such terms having anomalous final-state spectra.

APPENDIX C: THE FERMION–VECTOR-GLUON MODEL

We shall not present the detailed calculations in this model since they are rather lengthy. Instead we shall attempt to indicate the way in which they differ from the scalar case. Reference is given to previous literature which describes the complications of the introduction of spin.

The reason for considering the vector-exchange models in the first place is that, whereas adding an extra scalar exchange to a graph damps its asymptotic behavior by a factor of $1/s$ $(1/Q^2)$, adding an extra vector exchange does not change the asymptotic power.[36] Thus, our final-state-interaction graphs are known to scale *a priori*, up to possible powers of $\ln Q^2$. Such difference in behavior is brought about by the momentum-dependent numerators which appear in theories with spin.

The question of final-state distribution of partons in such a model is in essence rather similar to the scalar case. Studies of the ladder exchange by Cheng and Wu, Chang and Fishbane, and Kogut[37] show that the essential difference which the numerator factors make to such an exchange is that they allow only strong ordering of pairs of fermions rather than individual fermions. This occurs because the strong ordering of the two members of a pair involves fermion exchange, and thus damps the asymptotic behavior over the case with only vector exchange. As for the scalar case, a power of $\ln s$ arises from each strong ordering.

In our model (Fig. 21) the absence of such strong ordering of ladder rungs is forced upon us by the denominators of the sides of the ladder in exactly the same way as for the scalar case treated in Appendix A. Similar arguments extend to the Mandelstam graph of Fig. 24. The spectrum of final states is thus found to be the same as in the scalar case, with its leading parton, and target fragments, but no plateau or charge-exchange mechanism.

Of course, as indicated by previous authors, such a theory does not scale, since strong ordering of the transverse momenta can give powers of $\ln s$.[27,38] This behavior is suppressed by the Drell-Levy-Yan artifice of restricting the transverse momentum integrations. The theory then scales.

The annihilation processes in the cutoff vector-gluon model are related to those in the scalar case (Appendix D) in a similar manner. The final-state-interaction graphs now contribute asymptotically, but the spectrum shows the bunching of the scalar case.

Finally, we should make a few comments about minimally coupled massive vector-meson theories. Although such theories are not gauge-invariant, the Abelian vector field is coupled to a conserved current. This allows us to get many properties of gauge-invariant theories (renormalizability, Ward identities, etc.), but requires that we always deal with a set of diagrams which would preserve gauge invariance in a massless vector-meson theory. Our choice of diagrams is motivated by previous experience.

APPENDIX D: ANNIHILATION IN ϕ^3 THEORY

We consider the discontinuity of Fig. 26 in ϕ^3 theory. For convenience we restrict our calculation to scalar photons. We define the photon momentum to be $p + q$, where $p = (0, Q, \vec{0})$, $q = (Q, 0, \vec{0})$, and our components are $(+, -, \vec{1})$. Thus, $(p+q)^2 = Q^2$ as desired.

The ladder rungs each give a factor

$$\theta(k_i^0 - k_{i+1}^0)\delta((k_i - k_{i+1})^2 - m^2) . \tag{D1}$$

These lead, as in Appendix A, to the orderings

$$-Q < k_{n-} < k_{n-1\,-} < \cdots < k_{2-} < k_{1-} < 0 \tag{D2a}$$

and

$$0 < k_{n+} < k_{n-1\,+} < \cdots < k_{2+} < k_{1+} < Q . \tag{D2b}$$

Now let us consider the poles in the k_+ variable. We use the arguments of Appendix A to consider only contributions $\sim 1/Q^2$ from the k integration. (N.B., the two rung case is not included in this discussion.) The poles in k_+ are given by the following.

The pole in $[(k+q)^2 - m^2 + i\epsilon]^{-1}$ is at

$$k_+ = -Q + \frac{\vec{k}^2 + m^2 - i\epsilon}{k_-} , \tag{D3}$$

which is in the upper half plane for $k_- < 0$, and in the lower half plane for $k_- > 0$.

The pole in $[(k-p)^2 - m^2 + i\epsilon]^{-1}$ is at

$$k_+ = \frac{\vec{k}^2 + m^2 - i\epsilon}{k_- - Q} , \tag{D4}$$

which is in the upper half plane for $k_- < Q$, and in the lower half plane for $k_- > Q$.

The pole in $[(k_j + k)^2 - m^2 + i\epsilon]^{-1}$ is at

$$k_+ = -k_{j+} + \frac{(\vec{k} + \vec{k}_j)^2 + m^2 - i\epsilon}{k_- + k_{j-}} , \tag{D5}$$

which is in the upper half plane for $k_- < -k_{j-}$, and in the lower half plane for $k_- > -k_{j-}$. We note that (D2a) gives $0 < -k_{j-} < Q$.

Thus all poles are in the upper half k_+ plane for $k_- < 0$, and in the lower half plane for $k_- > Q$. So we have a contribution only for

$$0 < k_- < Q . \tag{D6}$$

We choose to close the contour in the lower half k_+ plane for $0 < k_- < \frac{1}{2}Q$, thus picking up poles (D3) and (D5) (provided $-k_{j-} < \frac{1}{2}Q$), but not (D4). For $\frac{1}{2}Q < k_- < Q$ we close the contour in the upper half plane picking up poles (D4) and (D5) (provided $-k_{j-} > \frac{1}{2}Q$), but not (D5).

Let us first consider the range $0 < k_- < \frac{1}{2}Q$. Evaluated at pole (D3) our denominators become

$$(k-p)^2 - m^2 + i\epsilon = -Q(k_- - Q) + (k_- - Q)\left(\frac{\vec{k}^2 + m^2 - i\epsilon}{k_-}\right) - \vec{k}^2 - m^2 + i\epsilon \tag{D7}$$

and

$$(k+k_i)^2 - m^2 + i\epsilon = (k_{i+} - Q)(k_- + k_{i-}) + (k_- + k_{i-})\left(\frac{\vec{k}^2 + m^2 - i\epsilon}{k_-}\right) - (\vec{k} + \vec{k}_i)^2 - m^2 + i\epsilon , \tag{D8}$$

while the measure for the k_- integration is dk_-/k_-. Now we examine our contributions to the integral.

Case 1: $k_- \sim Q$. Then the denominator (D7) gives a contribution $\sim Q^{-2}$. We must therefore require [from (D8)] that $k_{i+} = Q + O(1/Q)$ or $k_- \simeq -k_{i-}$, which can be avoided by deforming the k_- contour unless $-k_{i-} \simeq \frac{1}{2}Q$. However, for $k_- \simeq -k_{i-} \simeq \frac{1}{2}Q$ we see that dk_-/k_- will damp the contribution. Hence, we have only $k_{i+} \simeq Q + O(1/Q)$ (all i), and thus we have no strong ordering or powers of $\ln Q^2$.

Case 2: $k_- \sim Q^\alpha$, $-1 < \alpha < 1$. The denominator (D7) then produces a contribution $\sim Q^{-2}$. We see that (D8) requires that $k_{i+} - Q \lesssim \sim Q^{-\alpha}$, while $k_{i-} \lesssim \sim Q^\alpha$. The mass-shell conditions will then require that $k_{i+} = Q + O(Q^{-\alpha})$ and $k_{i-} \sim Q^\alpha$ for all i. Thus, we have no strong ordering or powers of $\ln Q^2$.

Case 3: $k_- \sim 1/Q$. The denominator (D7) will give a contribution $\sim Q^{-2}$. (D8) requires that $k_- + k_{i-} \sim 1/Q$ and hence $k_{i-} \sim 1/Q$. Therefore, we have no strong ordering or powers of $\ln Q^2$.

Case 4: Special case.

$$(\vec{k}^2 + m^2 - i\epsilon)/k_- \simeq Q . \tag{D9}$$

Hence,

$$k_- \simeq (\vec{k}^2 + m^2 - i\epsilon)/Q . \tag{D10}$$

Since the minimum value of (D10) is m^2/Q, we may deform our contour in a manner similar to Fig. 32. On such a contour, the difference between the two sides of (D9) is $\sim Q$, and we return to Case 3.

Evaluated at pole (D5) $(-k_{j-} < \frac{1}{2}Q)$ our denominators are

$$(k+q)^2 - m^2 + i\epsilon = (Q - k_{j+})k_- + k_-\left(\frac{(\vec{k} + \vec{k}_j)^2 + m^2 - i\epsilon}{k_- + k_{j-}}\right) - \vec{k}^2 - m^2 + i\epsilon , \tag{D11}$$

$$(k-p)^2 - m^2 + i\epsilon = -k_{j+}(k_- - Q) + (k_- - Q)\left(\frac{(\vec{k} + \vec{k}_j)^2 + m^2 - i\epsilon}{k_- + k_{j-}}\right) - \vec{k}^2 - m^2 + i\epsilon , \tag{D12}$$

$$(k+k_i)^2 - m^2 + i\epsilon = (k_{i+} - k_{j+})(k_{i-} + k_-) + (k_{i-} + k_-)\left(\frac{(\vec{k} + \vec{k}_j)^2 + m^2 - i\epsilon}{k_- + k_{j-}}\right) - (\vec{k}_i + \vec{k})^2 - m^2 + i\epsilon , \tag{D13}$$

and the measure is $dk_-/(k_- + k_{j-})$. The range of integration is $-k_{j-} < k_- < \frac{1}{2}Q$.

Case 1: $k_- \sim Q$. The contribution of (D11) and (D12) will decrease faster than $1/Q^2$ unless $k_{j+} \sim 1/Q$, when it is $\sim 1/Q^2$. Then (D13) requires that $k_{i+} \sim 1/Q$ or $k_- \simeq -k_{i-}$. This second point can be avoided unless $-k_{i-} \simeq \frac{1}{2}Q$ or $-k_{i-} \simeq -k_{j-}$. For the former the measure $dk_-/(k_- + k_{j-})$ damps the integral. For the latter (D12)$^{-1}$ behaves like $\sim Q^{-1}(k_- + k_{j-})$ and damps the integral. Thus $k_{i+} \sim 1/Q$ (all i), and there is no strong ordering to produce powers of $\ln Q^2$.

The other way of obtaining a contribution $\sim 1/Q^2$ is to require $k_{j+} = Q + O(1/Q)$. We see immediately (by symmetry) that this just requires $k_{i+} = Q + O(1/Q)$ (all i), and hence no strong ordering or powers of $\ln Q^2$.

Case 2: $k_- \sim Q^\alpha$ ($-1 \le \alpha < 1$). We note that this obtains only if $-k_{j-} \le \sim Q^\alpha$. The contribution of (D11) and (D12) damps faster than Q^{-2} unless $k_{j+} \le \sim Q^{-\alpha}$ (or $Q - k_{j+} \le \sim Q^{-\alpha}$), when this contribution $\sim Q^{-2}$. This requires that in (D13), that $k_{i-} \le \sim Q^\alpha$ and $k_{i+} \le \sim Q^{-\alpha}$ (or $Q - k_{i+} \le \sim Q^{-\alpha}$) for all i. The mass-shell conditions then demand that $k_{i-} \sim Q^\alpha$ and $k_{i+} \sim Q^{-\alpha}$ [or $k_{i+} = Q + O(Q^{-\alpha})$] for all i. Thus we have no strong ordering or powers of $\ln Q^2$.

Case 3: *Special case.*

$$k_{j+} \simeq \frac{(\vec{k} + \vec{k}_j)^2 + m^2 - i\epsilon}{k_- + k_{j-}} \,, \tag{D14}$$

i.e.,

$$k_- \simeq -k_{j-} + \frac{(\vec{k} + \vec{k}_j)^2 + m^2 - i\epsilon}{k_{j+}} \,. \tag{D15}$$

Subcase 1: $k_{j+} \sim 1/Q$ and thus $k_- = -k_{j-} + O(Q)$. Such a point can be avoided by $\sim Q$ (unless $k_- \simeq \frac{1}{2}Q$, where the measure damps the contribution), and thus we are back to Case 1.

Subcase 2: $k_{j+} \sim Q^{-\alpha}$ ($-1 < \alpha < 1$) *and thus* $k_- = -k_{j-} + O(Q^\alpha)$. Such a point can be avoided by $\sim Q^\alpha$, thus returning us to Cases 2 or 1.

Subcase 3: $k_{j+} \sim Q$, $k_{j+} \simeq xQ$, *say* ($x \le 1$). Thus $k_- = -k_{j-} + O(1/Q)$. The restriction on x enables us to avoid this point by at least m^2/Q. This returns us to one of the earlier cases.

The second contribution of the second region ($\frac{1}{2}Q < k_- < Q$) is obtained most easily by symmetry

from the first. To do this we define $\hat{k} = p - q - k$, $\hat{k}_i = -p + q - k_{n+1-i}$. Under this transformation, we merely invert the graph and thus find the same expression in terms of the variables $\hat{k}, \hat{k}_i$ as we had previously in terms of the variables k and k_i. The region $\frac{1}{2}Q < k_- < Q$ becomes $0 < \hat{k}_- < \frac{1}{2}Q$ and the upper-half k_+ plane becomes the lower-half $\hat{k}_+$ plane. Thus this second region gives exactly the same contribution as the first.

Hence, we see that the final state consists of one parton with $+$ momentum $\simeq Q$ and $-$ momentum $\sim 1/Q$, and an antiparton with $-$ momentum $\simeq Q$, and $+$ momentum $\sim 1/Q$. In addition, there is a bunch of partons whose $+$ momenta $\sim Q^{-\alpha}$ and whose $-$ momenta $\sim Q^\alpha$ ($-1 < \alpha < 1$) and whose sum of $+$ momenta $\sim Q^{-\alpha}$ and whose sum of $-$ momenta $\sim Q^\alpha$, as depicted in Fig. 29(a). We also have the degenerate cases ($\alpha = \pm 1$) where either one parton has $+$ momentum $\simeq Q$ and $-$ momentum $\sim 1/Q$, while the rest have $+$ momenta $\sim 1/Q$ and $-$ momenta $\sim Q$, or vice versa [Figs. 29(b), 29(c)].

The multiplicities in each case are easily seen to be finite.

We will now consider the second type of e^+e^- annihilation discontinuity depicted in Fig. 27. The graph itself is known to behave like $1/Q^2$ except for the lowest-order case,[21] which we shall ignore.

In order that the denominators of lines 2 and 3 should not damp the contribution, we must require that each have a momentum whose square is finite. For this to obtain requires line 1 to carry all except an amount $\sim 1/Q$ of either the plus or the minus component of the momentum $p + q$ and $\sim 1/Q$ of the other component. For convenience we consider line 1 to carry $+$ momentum $\simeq Q$ and hence $-$ momentum $\sim 1/Q$. Then lines 2 and 3 carry $-$ momentum $\simeq Q$ and $+$ momentum $\sim 1/Q$.

Since 2 and 3 have a finite invariant "mass," we can perform a z boost and obtain the situation where 2 and 3 have all momentum components finite. In this frame all the particles produced by 2 (or 3) will necessarily have finite momenta. Boosting back to the original frame, all these particles have $-$ momenta $\sim Q$ and $+$ momenta $\sim 1/Q$, and are produced with a finite multiplicity The same result is true for the case where the $+$ and $-$ components interchange roles. Hence, we populate the regions of Figs. 29(b) and 29(c).

[1] J. D. Bjorken, in *Proceedings of the International Symposium on Electron and Photon Interactions at High Energies, 1971*, edited by N. B. Mistry (Cornell Univ. Press, Ithaca, N. Y., 1972).

[2] S. Berman, J. D. Bjorken, and J. Kogut, Phys. Rev. D **4**, 3388 (1971).

[3] R. P. Feynman, *Photon Hadron Interactions* (Benjamin, New York, 1972), and talk presented at the Neu-

trino 1972 Conference, Balatonfüred, Hungary, 1972 (unpublished).

[4]M. Gronau, F. Ravndal, and Y. Zarmi, Nucl. Phys. B51, 611 (1973).

[5]Feynman has considered the influence the struck-quark quantum numbers may have on the distribution of quantum numbers among the final-state hadrons. (Cf. the second article of Ref. 3.) Similar dynamical ideas have been discussed by L. Susskind, Phys. Rev. D 6, 894 (1972).

[6]K. G. Wilson, Cornell University Report No. CLNS-131, 1970 (unpublished).

[7]L. Susskind, Phys. Rev. 165, 1535 (1968); L. Susskind, in Lectures in Theoretical Physics, edited by K. T. Mahanthappa and W. E. Brittin (Gordon and Breach, New York, 1969), Vol. XI D, p. 135. See also H. Bacry and N.-P. Chang, Ann. Phys. (N. Y.) 47, 407 (1968). For a recent review of infinite-momentum techniques and parton models see J. Kogut and L. Susskind, IAS report, 1972 (unpublished).

[8]Light-cone variables and infinite-momentum techniques have in fact been used from time to time in discussing multiperipheral models. See, for example, S. Fubini, in Strong Interactions and High Energy Physics, edited by R. G. Moorhouse (Plenum, New York, 1964), p. 259. The utility of this approach was also recognized independently by S.-J. Chang and R. Rajaraman, Phys. Rev. 183, 1517 (1969).

[9]The quantities a and b are related to the transverse and longitudinal size (appropriately defined) of a hadron in the infinite-momentum frame. They may, in fact, have weak (logarithmic) energy dependence. The inclusion of such dependence does not change any of the conclusions here.

[10]This argument should also serve as a warning for those more familiar with momentum-space discussions. For example, if ψ_i were replaced by a simple plane wave, then $|\psi_i|^2 = 1$, and the parton has equal probability of being everywhere at once. Then clearly the space-time argument given here does not go through. This option is, of course, unreasonable.

[11]For a review of multiperipheralism see G. F. Chew, in Summer School in Elementary Particle Physics, Theories of Strong Interactions at High Energies, held at Brookhaven National Laboratory, Upton, N. Y., 1969, edited by R. F. Peierls (Brookhaven National Laboratory, Upton, N. Y. 1970).

[12]R. P. Feynman, in High Energy Collisions, edited by C. N. Yang et al. (Gordon and Breach, New York, 1969); Phys. Rev. Lett. 23, 1415 (1969); unpublished.

[13]J. D. Bjorken, J. Kogut, and D. E. Soper, Phys. Rev. D 3, 1382 (1971).

[14]H. D. I. Abarbanel, M. L. Goldberger, and S. B. Treiman, Phys. Rev. Lett. 22, 500 (1969); G. Altarelli and H. R. Rubinstein, Phys. Rev. 187, 2111 (1969).

[15]Admittedly these features are much simpler to understand in an infinite-momentum frame for the proton, but we discuss them from this point of view just as a warmup for the calculations discussed in Sec. IV. One of us (J. K.) apologizes to infinite-momentum enthusiasts for his use of the lab frame.

[16]We consider ϕ^3 to exist in the perturbation-theory sense even though its energy spectrum makes it unphysical in the field-theory sense.

[17]This fact was realized by many authors, in particu-

lar, S. Adler and W.-K. Tung, Phys. Rev. Lett. 22, 978 (1969), and R. Jackiw and G. Preparata, Phys. Rev. Lett. 22, 975 (1969). More recent and elaborate investigations have been done by S.-J. Chang and P. M. Fishbane, Phys. Rev. D 2, 1084 (1970); and S. Blaha, ibid. 3, 510 (1971). Recently many of these results have been obtained by simpler means; see N. Christ, B. Hasslacher, and A. Mueller, Phys. Rev. D 6, 3543 (1972).

[18]In the sense of Weinberg S. Weinberg, Phys. Rev. 118, 838 (1960).

[19]S. D. Drell, D. J. Levy, and T.-M. Yan, Phys. Rev. 187, 2159 (1969); Phys. Rev. D 1, 1035 (1970); 1, 1617 (1970); T.-M. Yan and S. D. Drell, ibid. 1, 2402 (1970).

[20]These are S.-J. Chang's variables; see Chang and Fishbane (Ref. 17), and previous works by Chang.

[21]R. J. Eden, P. V. Landshoff, D. I. Olive, and J. C. Polkinghorne, The Analytic S-Matrix (Cambridge Univ. Press, Oxford, 1966).

[22]D. Amati, S. Fubini, and A. Stanghellini, Nuovo Cimento 26, 896 (1962); S. Mandelstam, Nuovo Cimento 30, 1127 (1963); J. C. Polkinghorne, Phys. Lett. 4, 24 (1963).

[23]H. Cheng and T. T. Wu, Phys. Rev. D 5, 3170 (1972). The conclusion that Regge residue functions fall quickly to zero as an external leg goes off shell was first realized in perturbation-theory calculations of G. Tiktopoulos and S. Treiman, Phys. Rev. 135, 711 (1964); 136, 1217 (1964). The H. Cheng and T. T. Wu formulation of this fact is particularly convenient for doing complicated calculations.

[24]S. Mandelstam, Nuovo Cimento 30, 1148 (1963).

[25]B. Hasslacher and D. K. Sinclair, Phys. Rev. D 3, 1770 (1971); and G. M. Cicuta and R. L. Sugar, ibid. 3, 970 (1971).

[26]S. D. Drell and T. D. Lee, Phys. Rev. D 5, 1738 (1972); T. D. Lee, ibid. 6, 1110 (1972).

[27]Such a model has been considered in detail by V. N. Gribov and L. N. Lipatov, Yad. Fiz. 15, 781 (1972) [Sov. J. Nucl. Phys. 15, 438 (1972)]; and by P. Fishbane and J. Sullivan, Phys. Rev. D 4, 2516 (1971). Similar calculations were carried out independently by A. Mason, University of Cambridge report, Cambridge, England, 1971 (unpublished). See also last of Ref. 17.

[28]P. M. Fishbane and J. D. Sullivan, Phys. Rev. D 7, 1879 (1973).

[29]I. S. Gerstein, K. Gottfried, and K. Huang, Phys. Rev. Lett. 24, 294 (1970).

[30]L.-P. Yu, Phys. Rev. D 4, 2775 (1971).

[31]F. M. Renard, Phys. Lett. 40B, 484 (1972).

[32]H. B. Nielsen and P. Olesen, Phys. Lett. 32B, 203 (1970); B. Sakita and M. Virasoro, Phys. Rev. Lett. 24, 1146 (1970).

[33]K. Johnson, Phys. Rev. D 6, 1101 (1972).

[34]S.-J. Chang and T.-M. Yan, Phys. Rev. D 4, 537 (1971); S.-J. Chang, T.-M. Yan, and Y.-P. Yao, ibid. 4, 3012 (1971).

[35]The volume of the unit hyperhedron in n-dimensional space is $1/n!$. The integration does not encounter the singularities of the strongly ordered case.

[36]H. Cheng and T. T. Wu, Phys. Rev. 186, 1611 (1969); S.-J. Chang and S. K. Ma, ibid. 188, 2385 (1969).

[37]H. Cheng and T. T. Wu, Phys. Rev. D 1, 2775 (1970); S.-J. Chang and P. M. Fishbane, ibid. 2, 1104 (1970); J. B. Kogut, ibid. 4, 3101 (1971).

[38]H. Cheng and T. T. Wu, Phys. Rev. Lett. 22, 1409 (1969).